Springer

Journal of Mechanical Science and Technology 23 (2009) 489~497

Journal of
Mechanical
Science and
Technology

www.springerlink.com/content/1738-494x
DOI 10.1007/s12206-009-0111-3

Evolution of micro solder joints under electromigration and elastic field †

Dongchoul Kim*

Department of Mechanical Engineering, Sogang University, Seoul, 121-742, Korea

(Manuscript Received July 25, 2008; Revised October 30, 2008; Accepted January 19, 2009)

Abstract

This paper proposes a three-dimensional model for the evolution of micro and sub-micro scale flip chip solder joints. The coupled mechanisms of electromigration and the corresponding stress gradient are incorporated into a diffuse interface model. A semi-implicit Fourier spectral method and the preconditioned biconjugate-gradient method are proposed for the computation to achieve high efficiency and numerical stability. Our simulations demonstrate dynamic evolution of solder joints and breakages at the interface on the cathode side. It is also shown that the dynamically incorporated stress gradient considerably affects the evolution of solder joints counteracting the electromigration process.

Keywords: Solder joint; Electromigration; Diffusion; Stress gradient; Diffuse interface model

1. Introduction

Solder joints in flip chip are the interconnection between a die and the package carrier. Due to the recent miniaturization of electronic devices, the diameter of a solder joint has been reduced from 100 μm to 50 μm and smaller. The average current density easily reaches 10^4 A/cm^2 and higher [1]. Under such high current density, electromigration in solder joints becomes a reliability concern for the high density microelectronic packaging with further miniaturization. The transport of momentum from electrons to atoms causes a flux of metal atoms to diffuse in the direction of the electron flow. At the sites of flux divergence, atoms will either deplete or accumulate, leading to the development of voids or hillocks which may cause failure of solder joints.

The reliability of solder joint under electromigration has been extensively studied in recent years [2-5]. From experiments during the operation of a real flip chip, it has been observed that void formation starts near the current crowding region of the solder contact, and spreads quickly across the contact area after nucleation [6]. Voids developed at the contact area reduce the contact cross-section. The associated increase of local current density further promotes electromigration and eventually leads to failure such as breakage. For quantitative study of the electromigration process in the solder bump, characteristics such as activation energy, threshold current density, effective charge numbers and electromigration rate have been measured by developed experimental techniques [7, 8]. Recently, it was observed that electromigration creates stresses that can retard electromigration [9-12].

To rigorously assess the reliability of solder joints, several approaches have been proposed to explain electromigration-induced damage of solder joints. While the proposed analyses have provided a valuable insight into the basic ideas of the electromigration-induced evolution of solder joints, it is still not clear how the solder bump evolves and leads to failure. Solder joints have been described by two-dimensional models, and voids at the contact region have been assumed to have a specifically designed shape and the evolving direction, which may lead inaccurate assessments [13, 14]. Furthermore, elec-

† This paper was recommended for publication in revised form by Associate Editor Jeonghoon Yoo

*Corresponding author. Tel.: +82 2 705 8643, Fax.: +82 2 712 0799
E-mail address: dckim@sogang.ac.kr

tromigration-induced stress has not been dynamically incorporated in the model. It is known that the accumulation of vacancies at the cathode can generate a tensile stress. A recent study showed that the build up of stress in a solder joint could have considerable effect [15].

We present a three-dimensional model for the evolution of flip chip solder joints. This model couples electromigration and stress gradient induced by the electromigration process. Previous two-dimensional models assumed preexisting voids that evolve following the guided evolving directions and shapes within steady solders. Our three-dimensional dynamic model allows us to investigate dynamic deformations of contact regions between evolving solders and flip chips. The failure time predicted by the two-dimensional model was calculated by the progress of a bar-shaped void at the contact region. It can have cases with definite deviations from the failure time calculated by the three-dimensional deformation of the contact region. Furthermore, a dynamically incorporated stress gradient in our model may affect the failure time since it can counteract or enhance the electromigration process with different progress in time. Considerable change of geometry in solder during evolution and multiple mechanisms in the system cause a computational challenge. This is addressed by employing a diffuse interface model with multiple concentrations. Three concentrations generate three different regions: flip chip, solder, and air. Each region with different material property evolves simultaneously. To efficiently resolve these complications, a robust numerical scheme is adopted.

2. Model

Here, we model the electromigration-induced evolution of a solder joint and consider a lead-free solder that has been currently replacing the conventional eutectic solders. Pure Sn solder may have the growth of Sn whiskers that probably give rise to a short circuit. It is considered that the compressive stress is the driving force for the growth of Sn whiskers [16, 17]. The compressive stress is generally induced by the diffusion of Cu into Sn and the formation of intermetallic compounds (IMC) [16, 17]. To prevent the growth of Sn whiskers, various methods have been investigated, such as annealing the Sn deposits, using a thick layer of Sn with larger grains, incorporating additives in the layer of Sn, and introducing a diffusion barrier [16-19]. Recently, it has been reported that a layer of Ni is an effective barrier to restrain the growth of Sn whiskers [20, 21]. The Ni layer can reduce Cu diffusion into the Sn layer, effectively preventing the formation of IMC. Hence, recently developed techniques allow us to assume that the effect of Sn whiskers can be neglected and focus on the electromigration process in studying the reliability of solder joints.

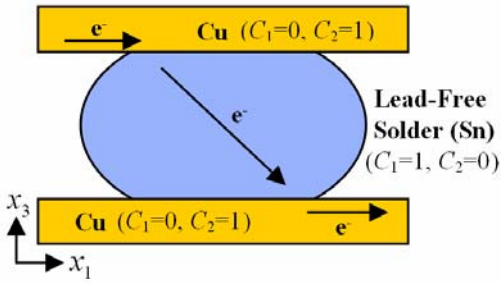

Fig. 1. A schematic drawing of a flip-chip solder joint. The two concentration fields, C_1 and C_2, represent a lead-free solder and plates, respectively.

Fig. 1 shows a schematic of the flip chip solder joint sandwiched between two copper plates. The solder may change its morphology by diffusion that is developed by electron wind and stress gradient. The arrows marked by e indicate the direction of electron flow. The system incorporates multiple kinetics and energetics, which are diffusion, electric field, elastic field, and surface tension. To efficiently present the morphological change of this system, a diffuse interface model is employed. We have demonstrated its efficiency and effectiveness in simulating dynamic evolutions of various nano/microstructures involving multiple mechanisms [22-25]. Here, three concentration fields, C_1, C_2, and C_3, are introduced to represent the lead-free solder, the copper plates, and air, respectively. We define a concentration C_1 by the volume fraction of the lead-free solder and a concentration C_2 by the volume fraction of the copper plates. Air in the domain is represented by C_3 which is $1-C_1-C_2$. The concentrations are regarded as spatially continuous and time-dependent functions, $C_1(x_1,x_2,x_3,t)$ and $C_2(x_1,x_2,x_3,t)$. For simplicity, we assume isotropic surface energy and diffusivity.

Following Cahn-Hilliard, the free energy of the system with multiple concentrations can be defined as

$$G=\int\left\{g_c(C_1,C_2)+h_{11}(\nabla C_1)^2\right.$$

$$+h_{22}\left(\nabla C_2\right)^2+h_{12}\left(\nabla C_1\nabla C_2\right)\Big\}dV\,. \quad (1)$$

The first term represents the chemical energy in the system. Other terms account for the interfacial energy between three components, where h_{11}, h_{22}, and h_{12} are material constants. Atoms diffuse in the solder bump from high chemical potential regions to low chemical potential regions, which causes the solder bump to change its shape. The corresponding driving forces for diffusion in the solder bump and the plates are attributed to the chemical potential by $\mathbf{F}_1^{chem}=-\nabla\mu_1^0$ and $\mathbf{F}_2^{chem}=-\nabla\mu_2^0$, respectively. The chemical potential is related to the free energy by $\mu_1^0=\delta G/\delta C_1$ and $\mu_2^0=\delta G/\delta C_2$. In an electric field, one driving force is attributed to the electron wind force. A mechanical stress gradient is also generated by the electromigration and it can counteract or enhance the electromigration process [26]. Thus, the total driving force can be expressed by $\mathbf{F}_1=\mathbf{F}_1^{chem}+\mathbf{F}_1^{elec}+\mathbf{F}_1^{elas}$ and $\mathbf{F}_2=\mathbf{F}_2^{chem}+\mathbf{F}_2^{elec}+\mathbf{F}_2^{elas}$, where $\mathbf{F}_1^{elec}$ and $\mathbf{F}_2^{elec}$, $\mathbf{F}_1^{elas}$ and $\mathbf{F}_2^{elas}$ are the driving force related with the electric field and elastic field, respectively. The total driving force leads to the atomic flux of $\mathbf{J}_1=M_1\mathbf{F}_1$ and $\mathbf{J}_2=M_2\mathbf{F}_2$. By combining with the mass conservation relation, $\partial C_1/\partial t+\nabla\cdot\mathbf{J}_1=0$ and $\partial C_2/\partial t+\nabla\cdot\mathbf{J}_2=0$, Cahn Hilliard equations are obtained as follows:

$$\frac{\partial C_1}{\partial t}=\nabla\left[M_1\left\{\nabla\left(\frac{\delta g_c}{\delta C_1}-2h_{11}\nabla^2C_1-h_{12}\nabla^2C_2\right)+\mathbf{F}_1^{elec}+\mathbf{F}_1^{elas}\right\}\right], \quad (2)$$

$$\frac{\partial C_2}{\partial t}=\nabla\left[M_2\left\{\nabla\left(\frac{\delta g_c}{\delta C_2}-2h_{22}\nabla^2C_2-h_{12}\nabla^2C_1\right)+\mathbf{F}_2^{elec}+\mathbf{F}_2^{elas}\right\}\right]. \quad (3)$$

The chemical energy with three components has been derived from the studies of two-phase solidification [27]:

$$\begin{aligned}g_c=f_0\Big[&\left\{C_1^2\left(1-C_1\right)^2+C_2^2\left(1-C_2\right)^2+C_3^2\left(1-C_3\right)^2\right\}\\&+a_1\frac{C_1^2}{4}\left\{15\left(1-C_1\right)\left(1+C_1-\left(C_3-C_2\right)^2\right)+C_1\left(9C_1^2-5\right)\right\}\\&+a_2\frac{C_2^2}{4}\left\{15\left(1-C_2\right)\left(1+C_2-\left(C_3-C_1\right)^2\right)+C_2\left(9C_2^2-5\right)\right\}\\&+a_3\frac{C_3^2}{4}\left\{15\left(1-C_3\right)\left(1+C_3-\left(C_1-C_2\right)^2\right)+C_3\left(9C_3^2-5\right)\right\}. \quad (4)\end{aligned}$$

By taking $a_1=a_2=a_3=1$ for simplicity and $C_3=1-C_1-C_2$, the chemical potentials are expressed by

$$\frac{\partial g_c}{\partial C_1}=f_0\left\{2\left(2C_1+C_2-1\right)\left(2C_1^2-2C_1+2C_1C_2-C_2+2C_2^2\right)\right\}, \quad (5)$$

$$\frac{\partial g_c}{\partial C_2}=f_0\left\{2\left(C_1+2C_2-1\right)\left(2C_1^2-C_1+2C_1C_2-2C_2+2C_2^2\right)\right\}. \quad (6)$$

One driving force for diffusion in the solder bump is attributed to the electron-wind force, which refers to the effect of the momentum exchange between the moving electrons and the ionic atoms and is described as

$$\mathbf{F}_1^{elec}=-f_1^e\nabla\phi\,,\quad \mathbf{F}_2^{elec}=-f_2^e\nabla\phi\,, \quad (7)$$

where $f_1^e=\left|e\right|Z_1^*/\Omega_1$ and $f_2^e=\left|e\right|Z_2^*/\Omega_2$. Ω_1 and Ω_2 are the atomic volume of tin and copper, respectively. Z_1^* and Z_2^* are the phenomenological effective valence of the atom of tin and copper, respectively. e is the charge of an electron. The negative signs in equations mean that the force is in the direction of the electron flow. Due to the conservation of electric charges and Ohm's law, the electric potential obeys the Laplace equation,

$$\nabla\cdot\left\{\xi\left(C_1,C_2\right)\nabla\phi\right\}=0\,, \quad (8)$$

where ξ is the conductivity of the media, which is linearly interpolated by that of the solder bump and the copper plates, namely, $\xi(C)=\xi_1C_1+\xi_2C_2$. This partial differential equation, together with boundary conditions, determines the electric potential.

Here the stress gradients resulting from electromigration are shown to produce an additional driving force, given by [28]

$$\mathbf{F}_1^{elas}=-f_1^a\Omega_1\nabla\sigma\,,\quad \mathbf{F}_2^{elas}=-f_2^a\Omega_2\nabla\sigma\,, \quad (9)$$

where $\sigma=trace\left(\sigma_{ij}\right)/3$ is the hydrostatic stress for diffusion through the bulk. This driving force, which is taken to be proportional to the gradient to the hydrostatic stress, works against the electrical current-induced mass flow; it leads to atomic backflow.

By normalization with the characteristic length, L_c, time, t_c, mobilities, M_{1c}, M_{2c}, electric potential, ϕ_c, and the hydrostatic stress, σ_c,

$$\frac{\partial C_1}{\partial t}=\nabla\left\{M_1\nabla\left(\mu_1^0-Ch_{11}^2\nabla^2C_1-\frac{1}{2}Ch_{12}^2\nabla^2C_2-A\phi+B\sigma\right)\right\}, \quad (10)$$

$$R_M\frac{\partial C_2}{\partial t}=\nabla\left\{M_2\nabla\left(\mu_2^0-Ch_{22}^2\nabla^2C_2-\frac{1}{2}Ch_{12}^2\nabla^2C_1-A\phi+B\sigma\right)\right\}, \quad (11)$$

where the chemical potentials are $\mu_1^0=\left(2C_1+C_2-1\right)\left(2C_1^2-2C_1+2C_1C_2-C_2+2C_2^2\right)$ and $\mu_2^0=\left(C_1+2C_2-1\right)\left(2C_1^2-C_1+2C_1C_2-2C_2+2C_2^2\right)$ The characteristic variables are $t_c=L_c^2/2M_{1c}f_0$, $Ch_{11}=h_{11}/L_c^2f_0$, $Ch_{12}=h_{12}/L_c^2f_0$, and $Ch_{22}=h_{22}/L_c^2f_0$. R_M is the ratio of the characteristic mobilities, $R_M=M_{1c}/M_{2c}$ and $A=\phi_c/2f_0$, $B=\sigma_c/2f_0$. Ch_{11}, Ch_{22}, and Ch_{12} are the Cahn numbers which represent the relative significance of the interface energy between materials.

The stress evolves along with electromigration. Here general equations which connect the stress and the diffusion equation are derived based on Sarychev's work [29]. We assume that the total strain tensor ε_{ij} has a purely elastic component ε_{ij}^{elas} and an inelastic component ε_{ij}^{elec} due to electromigration:

$$\varepsilon_{ij}=\varepsilon_{ij}^{elec}+\varepsilon_{ij}^{elas}. \quad (12)$$

We use the following equation for the evolution of the volume deformation ε_{ij}^{elec} due to electromigration [29]:

$$\frac{\partial\varepsilon_{kk}^{elec}}{\partial t}=\Omega\nabla\cdot\mathbf{J}. \quad (13)$$

In the solder region and the plate region, the inelastic component is represented by $\partial\varepsilon_{kk1}^{elec}/\partial t=\Omega\nabla\cdot\mathbf{J}_1$ and $\partial\varepsilon_{kk2}^{elec}/\partial t=\Omega\nabla\cdot\mathbf{J}_2$, respectively, where $\mathbf{J}_1=-M_1\left\{\nabla\left(\partial g_c/\partial C_1-2h_{11}\nabla^2C_1-h_{12}\nabla^2C_2\right)+\mathbf{F}_2^{elec}+\mathbf{F}_2^{elas}\right\}$ and $\mathbf{J}_2=-M_2\left\{\nabla\left(\partial g_c/\partial C_2-2h_{22}\nabla^2C_2-h_{12}\nabla^2C_1\right)+\mathbf{F}_2^{elec}+\mathbf{F}_2^{elas}\right\}$. We assume that Hook's law applies to the elastic deformation

$$\varepsilon_{ik}^{elas}=S_{iklm}\sigma_{lm}, \quad (14)$$

where S_{iklm} is the stiffness matrix. For isotropic materials, $S_{iklm}=-\delta_{ik}\delta_{lm}\left(v/E\right)+\left(\delta_{il}\delta_{km}+\delta_{kl}\delta_{im}\right)\left(1+v\right)/\left(2E\right)$. E is Young's modulus and v is the Poisson ratio. From Eq. (12) and (14), we have stress-strain relation:

$$\sigma_{ij}=-T\varepsilon_{kk}^{elec}\delta_{ij}+\lambda\varepsilon_{kk}\delta_{ij}+2\mu\varepsilon_{ij}, \quad (15)$$

where $T=\lambda+2\mu/3$ is the bulk modulus, $\lambda=vE/\left(\left(1+v\right)\left(1-2v\right)\right)$ and $\mu=E/\left(2\left(1+v\right)\right)$ are Lame's constants. We take E to have the form of $E\left(C_1,C_2\right)=E_1C_1+E_2C_2$, where E_1 and E_2 are material constants, and we assume v is a constant for simplicity. Lame's constants, λ and μ, consequently become functions of the concentrations. As derived by Sarychev, we take $\varepsilon_{kk}=\gamma\varepsilon_{kk}^{elec}$ for special situations including the strains being small and bulk diffusion considered. The hydrostatic stress for diffusion through the bulk has $\sigma=-\left\{2E\left(1+2\nu\right)\varepsilon_{kk}^{elec}\right\}/\left\{9\left(1-2\nu\right)\left(1-\nu\right)\right\}$. Thus, the stress fields in the solder region and the flip-chip region have the following relations.

$$\frac{\partial\sigma_1}{\partial t}=-\frac{2E_1}{9\left(1-v_1\right)}\Omega_1\nabla\cdot\mathbf{J}_1, \quad (16)$$

$$\frac{\partial\sigma_2}{\partial t}=-\frac{2E_2}{9\left(1-v_2\right)}\Omega_2\nabla\cdot\mathbf{J}_2. \quad (17)$$

By normalization,

$$\frac{\partial\sigma_1}{\partial t}=P_1f_1^a\Omega_1\nabla\left\{M_1\nabla\left(\mu_1^0-Ch_{11}^2\nabla^2C_1-\frac{1}{2}Ch_{12}^2\nabla^2C_2-A\phi-\frac{f_1^a\Omega_1}{2}\sigma\right)\right\}, \quad (18)$$

$$R_M\frac{\partial\sigma_2}{\partial t}=P_2f_2^a\Omega_2\nabla\left\{M_2\nabla\left(\mu_2^0-Ch_{22}^2\nabla^2C_2-\frac{1}{2}Ch_{12}^2\nabla^2C_1-A\phi-\frac{f_2^a\Omega_2}{2}\sigma\right)\right\}. \quad (19)$$

where $P_1=2E_1/\left\{9\left(1-v_1\right)\sigma_{c1}\right\}$ and $P_2=2E_2/\left\{9\left(1-v_2\right)\sigma_{c2}\right\}$.

3. Numerical implementation

The numerical approach needs to have a high spatial resolution to resolve the high order derivatives in the diffusion equation as well as the large gradients at the interface region. The approach should also be efficient and stable for the time integration, which is especially important for three-dimensional simulations. We propose an efficient semi-implicit Fourier spectral method for both high spatial resolution and fast computation. The central idea of the semi-implicit method is to treat the linear term implicitly and the nonlinear term explicitly to allow for larger time steps without losing numerical stability [30, 31]. In contrast, a fully implicit treatment yields expensive

schemes, while explicit discretization quickly leads to numerical instability or needs impractical time-step constraint,

$$\frac{\partial C_1}{\partial t} = 2\tau_1\nabla^2 C_1 + \tau_1\nabla^2 C_2 - Ch_{11}^2\nabla^4 C_1 - \frac{1}{2}Ch_{12}^2\nabla^4 C_2 + \left\{\nabla\cdot M_1\nabla\left(\mu_1^0 - Ch_{11}^2\nabla^2 C_1 - \frac{1}{2}Ch_{12}^2\nabla^2 C_2 - A\phi + B\sigma\right) - 2\tau_1\nabla^2 C_1 - \tau_1\nabla^2 C_2 + Ch_{11}^2\nabla^4 C_1 + \frac{1}{2}Ch_{12}^2\nabla^4 C_2\right\}, \quad (20)$$

$$R_M\frac{\partial C_2}{\partial t} = 2\tau_2\nabla^2 C_2 + \tau_2\nabla^2 C_1 - Ch_{22}^2\nabla^4 C_2 - \frac{1}{2}Ch_{12}^2\nabla^4 C_1 + \left\{\nabla\cdot M_2\nabla\left(\mu_2^0 - Ch_{22}^2\nabla^2 C_2 - \frac{1}{2}Ch_{12}^2\nabla^2 C_1 - A\phi + B\sigma\right) - 2\tau_2\nabla^2 C_2 - \tau_2\nabla^2 C_1 + Ch_{22}^2\nabla^4 C_2 + \frac{1}{2}Ch_{12}^2\nabla^4 C_1\right\}. \quad (21)$$

Note that stability is achieved in conjunction with the extrapolated Gear (SBDF) scheme for time integration. Among the second order multi-step methods, SBDF has the strongest high modal decay [32]. This provides the required damping for the very high frequencies in the diffusion equation without a harsh time-step constraint. Applying the scheme to the normalized diffusion equation, we obtain the following discretized form:

$$\frac{3}{2}C_1^{n+1} - 2C_1^n + \frac{1}{2}C_1^{n-1} = \Delta t\left(2\tau_1\nabla^2 C_1^{n+1} + \tau_1\nabla^2 C_2^{n+1} - Ch_{11}^2\nabla^4 C_1^{n+1} - \frac{1}{2}Ch_{12}^2\nabla^4 C_2^{n+1}\right) + 2P_1^n - P_1^{n-1}, \quad (22)$$

$$\frac{3}{2}C_2^{n+1} - 2C_2^n + \frac{1}{2}C_2^{n-1} = \frac{\Delta t}{R_M}\left(2\tau_2\nabla^2 C_2^{n+1} + \tau_2\nabla^2 C_1^{n+1} - Ch_{22}^2\nabla^4 C_2^{n+1} - \frac{1}{2}Ch_{12}^2\nabla^4 C_1^{n+1}\right) + 2P_2^n - P_2^{n-1}. \quad (23)$$

where

$$P_1^n = \Delta t\left\{\nabla\cdot M_1\nabla\left(\mu_1^{0n} - Ch_{11}^2\nabla^2 C_1^n - Ch_{12}^2\nabla^2 C_2^n/2 - E\phi + B\sigma\right) - 2\tau_1\nabla^2 C_1^n - \tau_1\nabla^2 C_2^n + Ch_{11}^2\nabla^4 C_1^n + Ch_{12}^2\nabla^2 C_2^n/2\right\}, \quad (24)$$

$$P_2^n = \left(\Delta t/R_M\right)\left\{\nabla\cdot M_2\nabla\left(\mu_2^{0n} - Ch_{22}^2\nabla^2 C_2^n - Ch_{12}^2\nabla^2 C_1^n/2 - A\phi + B\sigma\right) - 2\tau_2\nabla^2 C_2^n - \tau_2\nabla^2 C_1^n + Ch_{22}^2\nabla^4 C_2^n + Ch_{12}^2\nabla^2 C_1^n/2\right\}. \quad (25)$$

By applying the Fourier transform to Eqs. (22) and (23), we effectively perform calculations with

$$\hat{C}_1^{n+1} = \frac{1}{Det}\left\{L_4\left(2\hat{C}_1^n - \frac{1}{2}\hat{C}_1^{n-1} + 2\hat{P}_1^n - \hat{P}_1^{n-1}\right) - L_2\left(2\hat{C}_2^n - \frac{1}{2}\hat{C}_2^{n-1} + 2\hat{P}_2^n - \hat{P}_2^{n-1}\right)\right\}, \quad (26)$$

$$\hat{C}_2^{n+1} = \frac{1}{Det}\left\{-L_3\left(2\hat{C}_1^n - \frac{1}{2}\hat{C}_1^{n-1} + 2\hat{P}_1^n - \hat{P}_1^{n-1}\right) + L_1\left(2\hat{C}_2^n - \frac{1}{2}\hat{C}_2^{n-1} + 2\hat{P}_2^n - \hat{P}_2^{n-1}\right)\right\}, \quad (27)$$

where $L_1 = 3/2 + 2\tau_1\Delta tk^2 + Ch_{11}^2\Delta tk^4$, $L_2 = \tau_1\Delta tk^2 + Ch_{12}^2\Delta tk^4/2$, $L_3 = \tau_2\Delta tk^2/R_M + Ch_{12}^2\Delta tk^4/(2R_M)$, $L_4 = 3/2 + 2\tau_2\Delta tk^2/R_M + Ch_{22}^2\Delta tk^4/R_M$, $Det = L_1L_4 - L_2L_3$. The caret '^' stands for the Fourier Transform, and $k^2 = k_1^2 + k_2^2 + k_3^2$. The electric field is determined by $\nabla\cdot\{\xi(C_1, C_2)\nabla\phi\} = 0$, which can also be written as $\xi\nabla^2\phi + \nabla\xi\cdot\nabla\phi = 0$. We apply the second order discretization and compute the matrix with the preconditioned biconjugate gradient method [33]. The Jacobi preconditioner is adopted. The approach allows efficient computation of large 3D domains. The stress field in Eq. (18) and (19) can be numerically solved by following the same procedure with the numerical implementation of the diffusion equations.

In the following we outline the procedure to compute C_i^{n+1} from C_i^n. First, we compute the electric potential field ϕ^n that corresponds to the concentration distribution C_i^n. Then using the solution of ϕ^n, we compute $\left(\mu_i^c\right)^n$. We solve the evolution of the stress field σ^n due to electromigration. Using $\hat{C}_i^n$, $\hat{\phi}^n$, and $\hat{\sigma}^n$, we compute the convective Cahn-Hilliard equation in Fourier space to obtain $\hat{C}_i^{n+1}$. The new concentration C_i^{n+1} is obtained from $\hat{C}_i^{n+1}$ by the inverse Fourier transform. The procedure is repeated until a prescribed time.

4. Results and discussions

A series of simulations have been performed, which give a whole picture of the evolution process. Representative results are shown in Figs. (2)-(6). The calculation domain size is $70\times70\times50$. The diameter of the solder bump is 50, which corresponds to a physical diameter of 50 μm since the characteristic

length is taken to be 1 μm. The plates at the top and the bottom of the solder have a thickness of 5. Visualized three-dimensional graphs represent the solder surface and the plates by tracking where C_1 and C_2 have 0.5. Unless otherwise noted, the following material parameters are used in our simulations. Young's modulus of Cu is 130 GPa and that of Sn is 50 GPa. Poisson ratio of Cu and Sn is 0.34 and 0.36, respectively. Atomic volume of Cu is 7.1 cm^3/mol and that of Sn is 16.3 cm^3/mol. Diffusivity of Cu and Sn at 150 °C is around 10^{-12} cm^2/s and 1.3×10^{-10} cm^2/s, respectively.

Fig. 2 shows evolution sequences when the electric field is not applied and with the applied electric field. As shown in Fig. 2(a), when the Cahn numbers are assigned as $Ch_{11} = 1.0$, $Ch_{22} = 1.0$, and $Ch_{12} = 0.1$, which the surface energy between the solder and the plates is ten times smaller than that of solder and the plates, the simulation without an electric field shows reasonably maintained spherical shape of solder for a long time similar to physical observations. As the interface energy of the contact area between the solder bump and the plates becomes smaller than that of the solder and the plate, the solder bump tends to remain spherical. If the interface energy of the contact area becomes comparable to that of the solder bump, the contact area will increase and the solder bump will be cylindrical to reduce the total surface energy. The plates diffuse slowly and almost remain flat, while the solder bump undergoes morphological evolution since the diffusivity of Cu at 150 °C is much smaller than that of Sn. The morphology of the system becomes stable and maintains its shape for a long time. However, this stable morphology is disturbed by the electron flow. Then, the contact area between the solder bump and the top plate quickly decreases, which will cause the failure of the solder joint as shown in Fig. 2(b). Electron wind flows from the left of the top plate to the right of the bottom plate as shown in Fig. 1. The solder bump is subjected to a normalized electric potential of 1 that corresponds to the current density of 10^4 A/cm^2, which is typical in experiments.

The current crowding occurs at the contact interface between the top plate and the solder bump. From experiments, the formation of a void is observed at the current crowding region. In our simulation, the solder bump starts to break apart from the top plate at the left side of the solder bump in the downward electron flow. It is consistent with experimental observations in which a void tends to initiate where current-crowding occurs. When a void forms, it blocks the original electrical path and changes the current-crowding region to travel around the void. The growth of the void reduces the effective contact area at the interface region and increases the current density in the remaining contact area. This makes the current density higher and eventually causes circuit failure. In simulations, the contact area between the solder bump and the top plate decreases, while the contact area between the solder bump and the bottom plate increases. The shape of the solder also becomes flatter. The evolution sequence shows that the electron wind causes solder material to diffuse from cathode to anode.

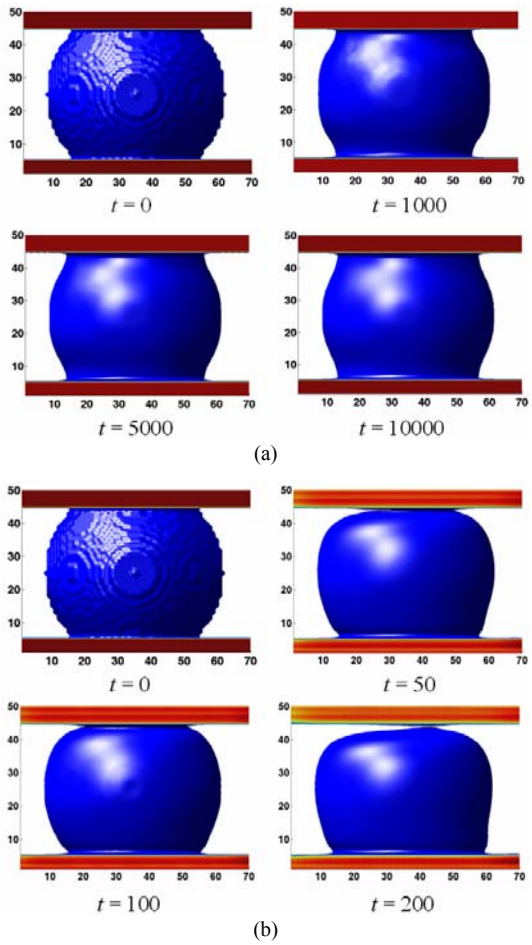

Fig. 2. The simulation results (a) without the applied electric field and (b) under the electric field. The applied electric field is A = 1.0 and the Cahn numbers are Ch_{11} = 1.0, Ch_{22} = 1.0, and Ch_{12} = 0.1.

In Fig. 3, the failure time is calculated by the area

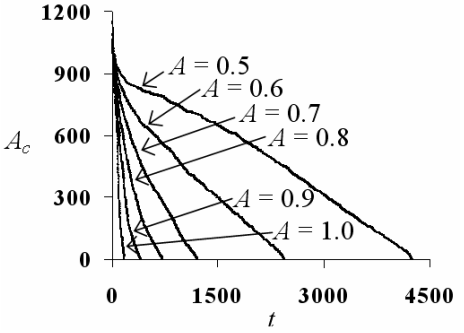

Fig. 3. The area of the contact region between the solder and the top plate (A_c) changes with different strengths of the applied electric fields (A). The Cahn numbers are $Ch_{11} = 1.0$, $Ch_{22} = 1.0$, and $Ch_{12} = 0.1$.

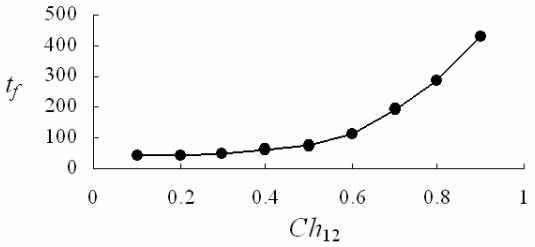

Fig. 4. The enhanced interface energy at the contact region induces the improved reliability of the solder joint. The failure time (t_f) is plotted as a function of time with the different Chan numbers (Ch_{12}).

of the contact region between the solder and the top plate with various strengths of the applied electric field. The failure time is almost exponentially decreased as the strength of the applied field increases, as shown in Fig. 3. When the normalized strength of the applied electric field reaches near 1, it is expected that the failure time will not be affected significantly by a stronger electric field under the present conditions of simulations. With the different conditions such as high temperature, the electromigration-induced diffusion can be aroused and the failure time may be decreased with the same electric field. Also, the more minimized solder joint will generate a higher electric current density, which will affect the failure time.

Fig. 4 shows the simulation results with the various interface energy of the contact region, which can be employed by the Ni layer or other material that is an effective barrier to restrain the growth of Sn whiskers [20, 21]. As shown in Fig. 4, the enhanced interface energy by the chemical manipulation improves the reliability of the solder joint as increasing the failure

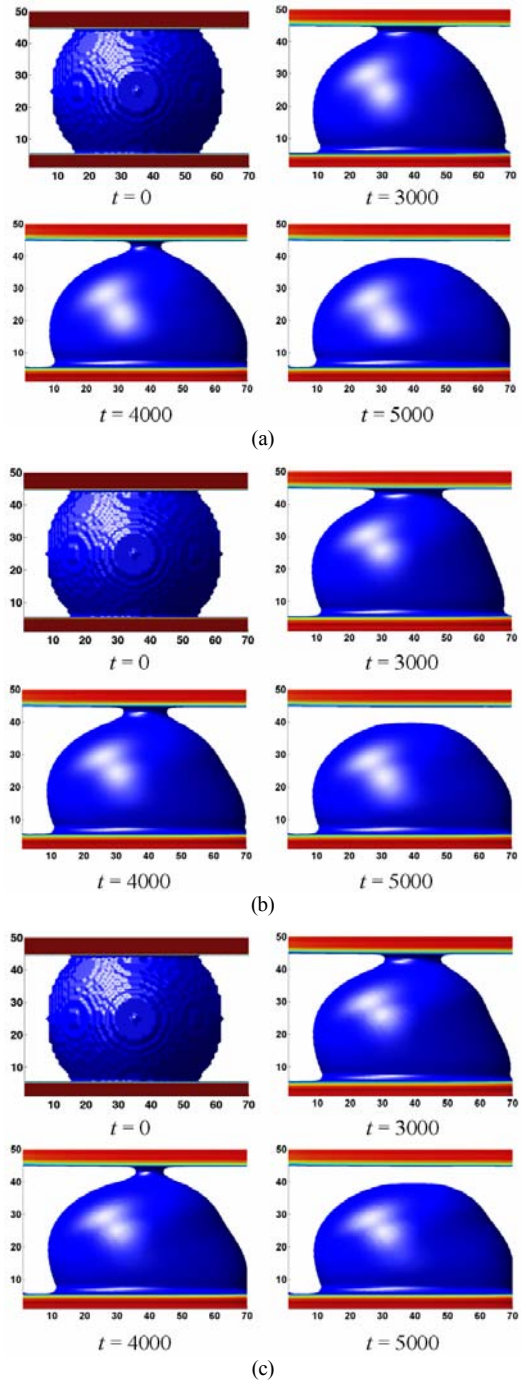

Fig. 5. The failure time is changed by the stress gradient. The stress gradient did not consider (a). The weighting factor of the stress gradient is (b) $B = 1.0$ and (c) $B = 2.0$. The applied electric field is $A = 0.5$ and the Cahn numbers are $Ch_{11} = 1.0$, $Ch_{22} = 1.0$, and $Ch_{12} = 0.1$.

time. These results suggest that we can investigate the effect of the chemically and geometrically designed

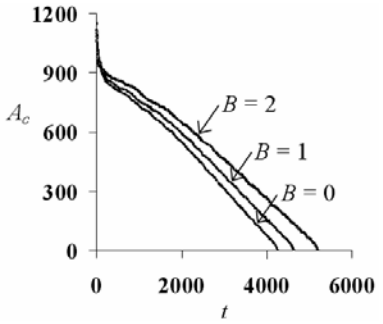

Fig. 6. The cross section areas of contact region between the solder and the flip-chip (A_c) are plotted. The applied electric field is $A = 0.5$. The Cahn numbers are $Ch_{11} = 1.0$, $Ch_{22} = 1.0$, and $Ch_{12} = 0.1$.

contact region on the reliability of the solder joint. The reliability of the solder joint considerably depends on the condition of the contact region where the failure happens. Thus, the chemical and geometrical manipulation to increase the interface energy will improve the reliability of the solder joint in addition to preventing Sn whiskers.

It has been observed that electromigration generates a stress gradient in the solder bump, and the simulation results incorporating the generated stress gradient are presented in Fig. 5. The applied electric field is $A = 0.5$. The stress gradient is not considered in Fig. 5(a). The weighting of the stress gradient on the evolution process is described by B which is 1 and 2 in Fig. 5(b) and (c), respectively. As shown in Fig. 5, the departing process of the solder bump from the top plate becomes slow as the effect of the stress gradient increases. Simulations with the electromigration-induced stress gradient show that the stress gradient counteracts the electromigration process. In Fig. 6, the failure time is calculated by the area of the contact region between the solder and the top plate with the stress gradient. In Fig. 6, the effect of the stress gradient on the failure time becomes significant as the effect of the stress gradient increases, which suggests that considering the coupled mechanism may be necessary to provide reliable predictions in some situations.

5. Conclusions

In a small scale flip chip solder joint, both electromigration and the corresponding stress gradient contribute to the mass transport of a solder bump. We model the coupled mechanism in electromigration in a continuum space. The three-dimensional model and computational approach proposed in this paper allow for a detailed study of the evolution process of the solder joint. The simulations show that the solder bump starts to break apart from the current-crowding region, and the failure time significantly decreases as the strength of the applied electric field increases. The results incorporating the stress gradient indicate that the generated stress gradient considerably influences the evolution of solder joints counteracting the electromigration process.

Acknowledgment

This work was supported by the Sogang University Research Grant of 2007118.

References

[1] K. N. Tu, Recent advances on electromigration in very-large-scale-integration of interconnects, *J. Appl. Phys.* 94 (9) (2003) 5451-5473.

[2] W. J. Choi, E. C. C. Yeh, et al., Mean-time-to-failure study of flip chip solder joints on Cu/Ni(V)/Al thin-film under-bump-metallization, *J. Appl. Phys.* 94 (9) (2003) 5665-5671.

[3] Y. H. Hsiao, Y. C. Chuang, et al., Prevention of electromigration-induced Cu pad dissolution by using a high electromigration-resistance ternary Cu-Ni-Sn layer, *Script. Mater.* 54 (4) (2006) 661-664.

[4] T. Y. Lee, K. N. Tu, et al., Electromigration of eutectic SnPb and $SnAg_{3.8}Cu_{0.7}$ flip chip solder bumps and under-bump metallization, *J. Appl. Phys.* 90 (9) (2001) 4502-4508.

[5] J. W. N. K. W. Paik, J. O. Suh, et al., Mechanism of electromigration-induced failure in the 97Pb-3Sn and 37Pb-63Sn composite solder joints, *J. Appl. Phys.* 94 (12) (2003) 7560-7566.

[6] E. C. C. Yeh, W. J. Choi, et al., Current-crowding-induced electromigration failure in flip chip solder joints, *Appl. Phys. Lett.* 80 (4) (2002) 580-582.

[7] Y. T. Yeh, C. K. Chou, et al., Threshold current density of electromigration in eutectic SnPb solder, *Appl. Phys. Lett.* 86 (20) (2005) 203504.

[8] C. Basaran, H. Ye, et al., Failure modes of flip chip solder joints under high electric current density, *J. Elect. Pack.* 127 (2) (2005) 157-163.

[9] I. A. Blech and C. Herring, Stress generation by electromigration, *Appl. Phys. Lett.* 29 (3) (1976) 131-133.

[10] I. A. Blech, Electromigration in thin aluminum films on titanium nitride, *J. Appl. Phys.* 47 (4) (1976) 1203-1208.
[11] I. A. Blech and K. L. Tai, Measurement of stress gradients generated by electromigration, *Appl. Phys. Lett.* 30 (8) (1977) 387-389.
[12] H. Ye, D. C. Hopkins, et al., Measurement of high electrical current density effects in solder joints, *Microelec. Relia* 43 (12) (2003) 2021-2029.
[13] L. Zhang, S. Ou, et al., Effect of current crowding on void propagation at the interface between intermetallic compound and solder in flip chip solder joints, *Appl. Phys. Lett.* 88 (1) (2006) 012106.
[14] S. W. Liang, Y. W. Chang, et al., Effect of three-dimensional current and temperature distributions on void formation and propagation in flip-chip solder joints during electromigration, *Appl. Phys. Lett.* 89 (2) (2006) 022117.
[15] H. Ye, C. Basaran, et al., Deformation of solder joint under current stressing and numerical simulation, *Int. J. Sol. Struct.* 41 (18-19) (2004) 4939-4958.
[16] K. N. Tu, C. Chen, et al., Stress analysis of spontaneous Sn whisker growth, *J. Mater. Sci. Mater. Electron.* 18 (1-3) (2007) 269-281.
[17] S. C. Hsu, S. J. Wang, et al., Effect of Cu content on interfacial reactions between Sn(Cu) alloys and Ni/Ti thin-film metallization, *J. Electron. Mater.* 32 (11) (2003) 1214-1221.
[18] H. Yu, V. Vuorinen, et al., Solder/substrate interfacial reactions in the Sn-Cu-Ni interconnection system, *J. Electron. Mater.* 36 (2) (2007) 136-146.
[19] H. J. Kao, W. C. Wu, et al., Effect of Cu additives on Sn whisker formation of Sn(Cu) finishes, *J. Electron. Mater.* 35 (10) (2006) 1885-1891.
[20] W. K. Choi, S. K. Kang, et al., A study of the effects of solder volume on the interfacial reactions in solder joints using the differential scanning calorimetry technique, *J. Electron. Mater.* 31 (11) (2002) 1283-1291.
[21] W. J. Choi, T. Y. Lee, et al., Tin whiskers studied by synchrotron radiation scanning X-ray microdiffraction, *J. Electron. Mater.* 51 (20) (2003) 6253-6261.
[22] D. Kim and W. Lu, Three-dimensional model of electrostatically induced pattern formation in thin polymer films, *Phys. Rev. B* 73 (3) (2006) 035206.
[23] D. Kim and W. Lu, Creep flow, diffusion, and electromigration in small scale interconnects, *J. Mech. Phys. Solids* 54 (12) (2006) 2554-2568.
[24] W. Lu and D. Kim, Engineering nanophase self-assembly with elastic field, *Acta. Mater* 53 (13) (2005) 3689-3694.
[25] W. Lu and D. Kim, Patterning nanoscale structures by surface chemistry, *Nano Lett.* 4 (2) (2004) 313-316.
[26] C. Basaran, M. Lin, et al., A thermodynamic model for electrical current induced damage, *Int. J. Sol. Struct.* 40 (26) (2003) 7315-7327.
[27] R. Folch and M. Plapp, Quantitative phase-field modeling of two-phase growth, *Phys. Rev. E* 72 (2) (2005) 011602.
[28] C. Herring, Diffusional viscosity of a polycrystalline solid, *J. Appl. Phys.* 21 (5) (1949) 437-445.
[29] M. E. Sarychev, Y. V. Zhitnikov, et al., General model for mechanical stress evolution during electromigration, *J. Appl. Phys.* 86 (6) (1999) 3068-3075.
[30] W. Lu and Z. Suo, Dynamics of nanoscale pattern formation of an epitaxial monolayer, *J. Mech. Phys. Solids* 49 (9) (2001) 1937-1950.
[31] J. Zhu, L.-Q. Chen, et al., Coarsening kinetics from a variable-mobility Cahn-Hilliard equation: Application of a semi-implicit Fourier spectral method, *Phys. Rev. E* 60 (4) (1999) 3564-3572.
[32] U. M. Ascher, S. J. Ruuth, et al., Implicit-explicit methods for time dependent partial differential equations, *SIAM J. Numer. Annal.* 32 (3) (1995) 797-823.
[33] G. H. Golub and C. F. V. Loan, *Matrix computation*, Johns Hopkins University Press, Baltimore, (1989).

Dongchoul Kim received a B.S. degree in Mechanical Engineering from Yonsei University in 2000. He then went on to receive his M.S. and Ph.D. degrees from The University of Michigan in 2003 and 2005, respectively. Dr. Kim is currently an Assistant Professor at the School of Mechanical Engineering at Sogang University in Seoul, Korea. His research interests are in the area of computational analysis of micro/nanostructures.